Power-free contact lens for glucose sensing

*Zongkang Li[1], Jeonghun Yun[1], Xiaoya Li[1], Moobum Kim[1], Jia Li[2], Donghoon Lee[1], Angyin Wu[1], Seok Woo Lee[1,2]**

[1]School of Electrical and Electronic Engineering, Nanyang Technological University, Singapore 639798, Singapore
[2]Rolls-Royce@NTU Corporate Lab, Nanyang Technological University, Singapore 639798, Singapore
* Corresponding author. Email: sw.lee@ntu.edu.sg

Keywords: wearable devices, smart contact lens, power-free, color change, glucose sensing

Recent advances in wearable devices have enabled noninvasive monitoring for healthcare applications. Smart contact lenses have gained substantial attention for medical diagnosis through the analysis of vital signs in tear fluids. However, previous studies have mostly focused on designs embedded with electronic devices or antennas for wireless transmission, which are power-intensive and require external receivers around the ocular system. Here, we report a power-free smart contact lens for noninvasive glucose sensing according to the color changes of multiple electrochromic electrodes to achieve direct data transmission without the external wireless system. The device detected various glucose concentrations, from the ordinary range (0.16–0.5 mM) to abnormally high concentrations (0.9 mM). The multi-electrode design exhibited acceptable accuracy, with a correlation coefficient r = 0.99543 to the controlled sample, and allowed low-glucose detections with concentrations down to 0.05 mM. The device showed good reproducibility, with standard deviations of determined glucose levels of 0.0462 and 0.025 for four continuous cycles and for an interval of several days, respectively. We believe that the reported smart contact lens has the potential for daily health monitoring by ordinary users without a power supply and external devices. Its simple electronics-free structure will allow for immediate application to the market with cost-effective manufacturing.

1. Introduction

Biomarker levels are essential indicators of overall health and body functions. Glucose, sourced from dietary intake and cellular metabolism, is a biologically essential molecule

associated with diabetes mellitus. Diabetes, an incurable disease, has been proven to be accompanied by critical complications such as micro- and macrovascular damage, cystic fibrosis, tuberculosis, and heart disease [1, 2], thus, its early diagnosis has become essential in medical treatments. Currently, the glucose levels of diabetes patients are commonly monitored via analysis of a capillary blood sample (i.e., blood sample collected via finger pricking) with a glucometer [3, 4]. However, this process is painful and inconvenient, and the effectiveness of the sensor depends on strict compliance. Recent efforts to develop flexible electronic devices with excellent biocompatibility and mechanical properties have led to the development of noninvasive health monitoring approaches supported by wearable devices for health management and early disease diagnosis [5, 6]. The wearable sensing of physiological signs and metabolites from individuals shows great potential for health monitoring at molecular levels [7]. Based on this innovation, wearable devices have been successfully applied in medical examinations including glucose sensing for disease diagnosis [5, 8, 9].

As one promising example of wearable healthcare devices, smart contact lenses have gained extensive attention owing to their ability to provide direct physiological information. Tear fluids comprise numerous detectable biomarkers, like glucose, which are closely correlated with blood composition [10]. Therefore, sensor-equipped smart contact lenses can provide reliable information via the analysis of biological signs from tears for disease treatments [11-14]. However, current studies have heavily relied on various power-consumable devices, such as electronic devices and integrated chips [15]. Owing to the extremely high safety requirement of eye environments, conventional batteries for epidermal wearable devices are incompatible with eye physiology in terms of toxicity, flexibility, heat, and area and can contribute to eye injuries [16, 17]. Biofuel cells have been studied as an alternative solution but are characterized by low power output [18, 19]. Recently, most smart contact lenses have used wireless power transmission technologies such as near-field communication (NFC) [20, 21]. To

achieve higher transmission efficiencies, antennas designed for wireless power transmission need to work at high frequencies; however, heat generation may pose a threat to the eyeballs.

In addition, most current smart contact lenses require the external receiver within effective distances, leading to inconvenience during the operation. Moreover, wireless data transmission requires significant power consumption, which is ~60 times that consumed by other embedded electronic components [14].

To tackle the issues of power supply and power-hungry data transmission for smart contact lenses, electrochromic systems characterized by visible color changes have been studied for direct signal transfer to the user [22] and the passive detection of biomarkers, including glucose level [23, 24]. However, the reported lenses exhibited a detection limit of 1.4 mM in glucose sensing [23]. Jeon et al. developed an optimal monitoring system in the contact lens for glucose sensing with an improved detection limit of 0.1 mM [24]; however, the embedded nanoparticles for color change were the cerium oxide nanoparticles (CNPs), which might react with disturbance components in tears like the ascorbic acid, which exhibits a comparable color change to that for glucose sensing [25]. Moreover, the biological toxicity of CNPs is still controversial [26]. Additionally, the reusability of the chromic sensor has not been investigated in most studies.

As one of the promising electrochromic electrode materials, Prussian blue (PB) has been widely studied and applied for enzyme-based glucose sensing because of its intrinsic peroxidase-like catalytic activity and fast reactions with hydrogen peroxide (H_2O_2) [27-30]. Here, we report a power-free contact lens glucose sensor consisting of electrodeposited PB electrodes with glucose oxidase (GOX) for selective glucose sensing and direct result indication via color variations of PB electrodes without external wireless transmission. A multi-electrode design and machine learning enabled wide-range and precise glucose detection. The proposed power-free contact lens achieved a low detection limit (0.05 mM) and the re-usability of the lens has been demonstrated as well.

Figure 1a illustrates the glucose sensing principle of the power-free smart contact lens. The smart contact lens was based on a hydrogel-covered 3D-printed structure and consisted of electrochromic electrodes, enzymes, and Nafion. At the initial state, the electrode of the lens occurred as Prussian White (PW), which is the reduced form of PB and appears transparent. In the presence of glucose, the electrodes were oxidized to PB, accompanied by an obvious color change from transparent to blue. Power sources and associated electronic components were thus eliminated. Photographs of the smart contact lens at the initial state and after glucose detection were captured for comparison to eliminate the error caused by pristine color differences between distinct lenses. The color change depended on both the tear glucose levels and the PB electrode thickness. The color change could be visibly recognized for instant glucose level estimation, which is helpful for the immediate determination of safe levels, and image processing was conducted via machine learning for precise glucose level detection.

The electrochemical mechanism of glucose detection is illustrated in Figure 1b. The immobilized GOX functioned as a catalyst, which catalyzes the oxidation of glucose to gluconic acid and H_2O_2 in the presence of oxygen. The generated H_2O_2 then oxidized the electrochromic material from the reduced state (PW) to the oxidized state (PB) through the transfer of cations (sodium ions, Na^+, and potassium ions, K^+), accompanied by an observable color change from transparent to blue during the electrochemical redox reaction. Since the glucose concentration controlled the kinetics of oxidation of PB, a higher glucose level resulted in a greater PB color change for the same reaction time (Figure 1b). Although H_2O_2 is considered corrosive, it usually causes severe damage at high concentrations. As the generated H_2O_2 from the enzymatic reactions in tears are at low concentrations and reacts with PB immediately upon contact, the potential threats posed by the generated H_2O_2 in the eyes can be considered negligible.

Because all of the required cations (Na^+ and K^+) for the PB reactions are contained in tears, additional electrolytes are not required. Characterization of the PB thin film confirmed the desired chemical reaction of PB in tear-like solutions (Figure S1). Moreover, PB has been

proven as a biocompatible and safe electrode material with stable electrochemical performance in the eyes [16, 31].

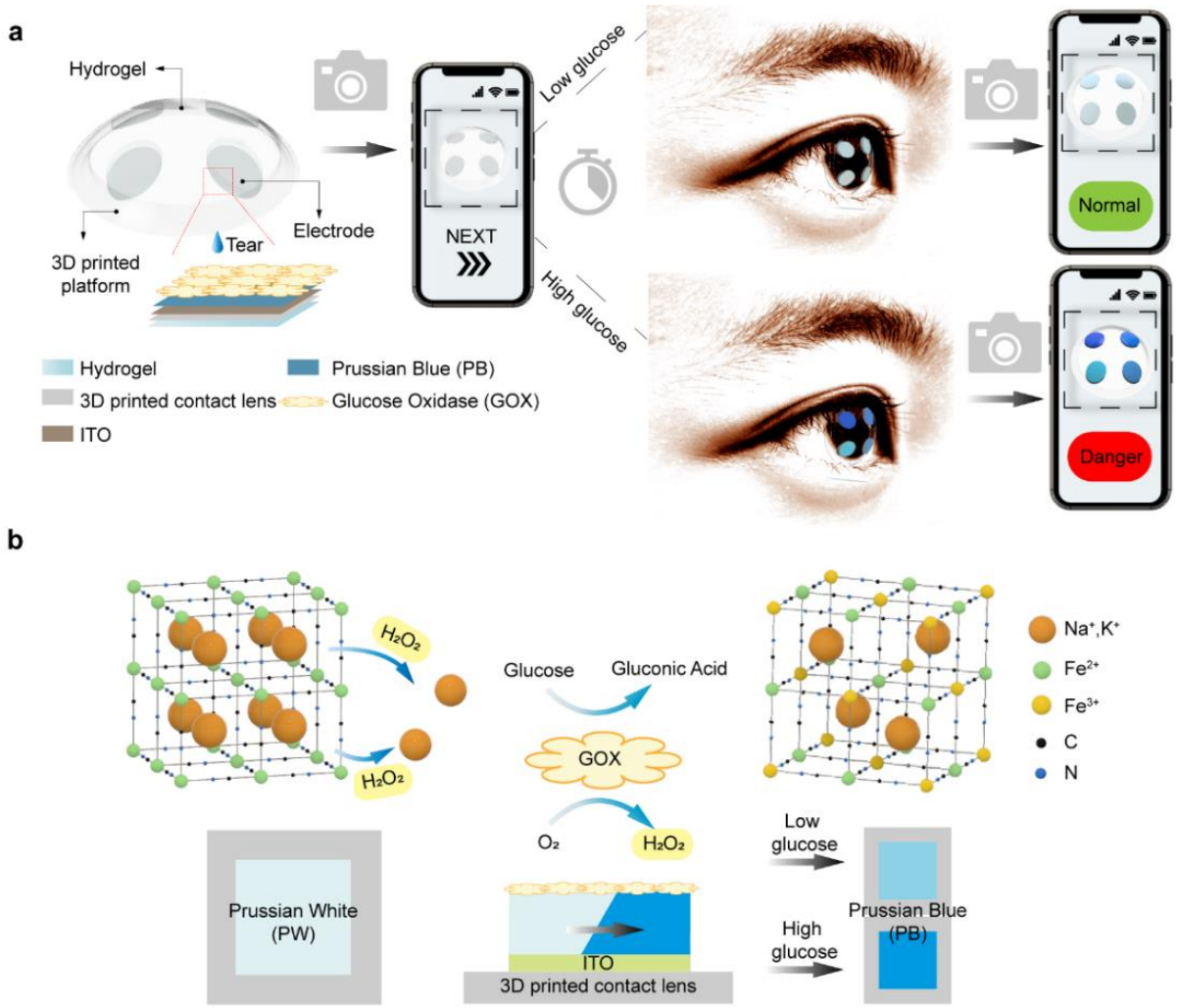

Figure 1. Power-free smart contact lens system for glucose detection. **a)** Power-free contact lens working principle. The initialized lens is first captured with the camera, followed by putting in eyes for certain-time processing. Then the lens after the application is captured for later comparisons with the initial lens to examine the color change and glucose status. The captured photos are computationally processed to examine the color change. Results for both low and high glucose concentrations are illustrated. **b)** Electrochemical reactions mechanism during color changes. The PW is oxidized to PB by H_2O_2 generated catalytic reaction of GOX and glucose, accompanying ions transfer and color change from transparent to blue. Different glucose concentrations result in different color variations as illustrated.

2. Results

2.1. Fabrication and optical characteristics of designed contact lens

Figure 2a shows the fabrication process of the power-free smart contact lens. The "Clear V4" substrate was fabricated using a digital light processing-based 3D printer according to the meniscus of the contact lens. Indium tin oxide (ITO, 250 nm thick) and PB were deposited on the substrate via sputtering and electrodeposition, respectively. The thickness of PB on each circular electrode varied from 144 to 1082 nm. Afterward, GOX was immobilized on the PB electrode surface for selective glucose sensing, followed by Nafion coating to protect the electrode materials from OH^- damage during glucose detection [32-34]. Finally, the contact lens was placed into a hemispheric lab-made mold for polymerization of the hydrogel solution under 365 nm ultraviolet (UV) light to complete the fabrication. The as-fabricated contact lens was designed with sufficient transparent space at the center to provide clear views without any vision block regardless of the wearer's pupil size (Figure 2b).

Transmittance tests of PB electrodes at different potentials were conducted to demonstrate the color change (Figure 2c). The transmittance located between wavelengths of 620 and 700 nm that correspond to the greatest absorption of the blue color was studied. The minimum transmittance of the PB electrode continuously decreased from 68.24% to 37.93% at 696.33 nm with increases in potential from 0 to 0.5 V, indicating deeper blue appearances observed in PB electrodes as potential increased. Although transmittance can be used as an indicator of color variations, it requires specific equipment like a UV–vis spectrophotometer, which is not accessible in practical applications. By contrast, color analysis in color space can be conducted easily via image processing using mobile phones. Here, we applied CIELAB color space (Supplementary Text CIELAB color space and Figure S2) and the parameters of the color space at the different potentials of PB were measured (Figure 2d). There are three different parameters, L*, a*, and b*, representing lightness, red and green, yellow and blue, respectively. As the potential increased, b* of the CIELAB color space decreased continually, from −14.78 at 0 V

to −28.11 at 0.5 V, while L* and a* remained approximately the same values at all potentials. The variation of b* during the change of potential agreed well with that of the transmittance measured at 696.33 nm; hence, b* can represent the color of PB electrodes. The b* of the pristine PB electrodes and GOX-immobilized PB electrodes were compared (Figure S3). Despite the slight shifts in b* attributed to the light-yellow color of GOX immobilization, b* of the PB electrodes of various thicknesses were still distinct and could be applied to indicate color degrees.

Comparisons under three PB electrode conditions (glucose with GOX, glucose without GOX, and no glucose with GOX) were conducted to confirm the glucose detection ability of PB electrodes with GOX, as illustrated in Fig. 2E. Instead of the absolute value of b*, the difference between the initial and final b* (Δb*) was evaluated in the following experiments to eliminate errors in the pristine b* of different contact lenses caused during the fabrication process. The PB electrodes in glucose with GOX exhibited a large saturated Δb* five minutes after the glucose observation in a tear-like solution with 0.9 mM glucose with a value of 15, as indicated by the blue curve of Figure 2e. However, the pristine PB electrode in the 0.9 mM glucose solution and the GOX-immobilized PB electrode in the non-glucose solution exhibited only a third of the above Δb* (Figure 2e, orange and black curves, respectively). The occurrence of a small Δb* was due to PB self-oxidation, which happens spontaneously with dissolved oxygen in water [35]. Since the rate of PB self-oxidation was much slower than the reactions between H_2O_2 and PW, the influences of PB self-oxidation during a short detection time (i.e., 20 minutes) were negligible. The inset photographs in Fig. 2e showed electrodes at the initial state and after 20 minutes under different conditions. Contact lens users could roughly detect the glucose levels with their bare eyes via color change, and accurate glucose levels could be detected via the CIELAB color space-based analysis. Moreover, the ability of the sensor in glucose sensing was verified by the amperometric current response (Figure S4b).

The cyclic voltammetry (CV) results of the PB electrode before and after GOX immobilization, as well as after glucose sensing in tear-like solutions illustrated consistent electrochemical properties of the designed glucose sensor (Figure 2f). The slight decrease in the peak current in the GOX-immobilized electrode compared with that of the pristine PB electrode was possibly caused by the sluggish diffusion of Na^+ and K^+ from the bulk solution in the presence of GOX and Nafion layers. While the peak potential shifts in the electrode after GOX immobilization and glucose sensing compared with the pristine PB electrode may be attributed to the disturbance in diffusion caused by the GOX-Nafion coated layers [36] and the loss of the PB activity after reacting with H_2O_2 [37], respectively.

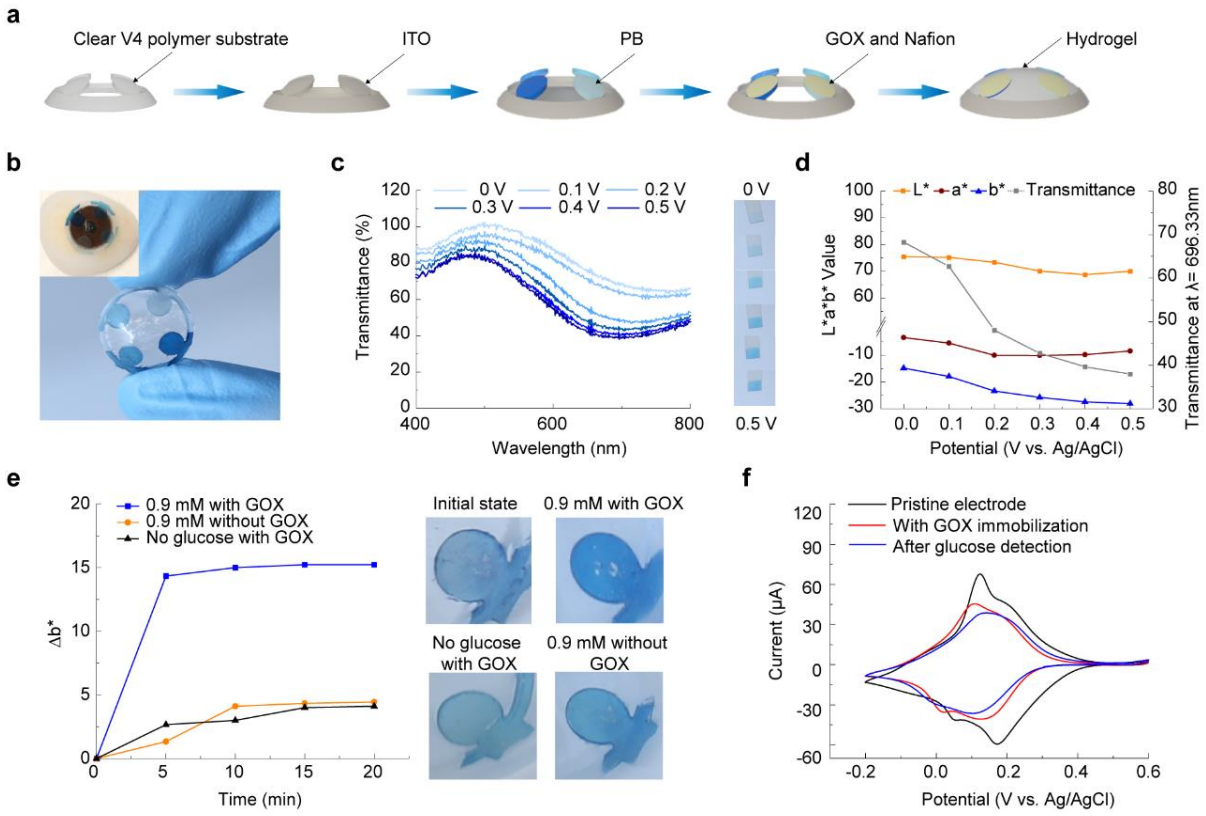

Figure 2. Fabrication and characterization of smart contact lenses. a) Fabrication. The power-free contact lens was built on the hydrogel-covered "Clear V4" polymer substrate, covered by ITO, PB electrode material, GOX enzyme solution, and Nafion layers sequentially. And finally, a hydrogel solution was applied to form the complete lens. **b)** Photographs of power-free smart contact lenses hold in hand and put above the artificial eye. **c)** Transmittance

measurement of PB thin films on the ITO plat film in tear-like solution (0.145 M NaCl and 0.024 M KCl) was conducted from 0.0 V to 0.5 V (vs. Ag/AgCl) with the increment of 0.1 V. **d)** Transmittance and CIELAB color space measurement results of the PB electrodes. **e)** Δb* and corresponding images of PB electrodes with GOX in 0.9 mM glucose solution (blue line), in 0.9 mM glucose solution without GOX (orange line), and in the non-glucose tear-like solution with GOX (black line). **f)** The CV curves of PB electrodes of pristine (black), after GOX immobilization (red), and after glucose detection (blue) in a tear-like solution.

2.2. Biosensing chemistry and characterization

The analytical responses of a single PB electrode with two different thicknesses were investigated in a tear-based solution containing various glucose concentrations by tracking Δb* tracking per 5 minutes. The thin PB electrode (144 nm thick) exhibited excellent capability, with remarkable distinct Δb* values, in the detections of solutions with low glucose concentrations, while significant overlaps in Δb* occurred at glucose concentrations greater than 0.3 mM (**Figure 3**a). At low glucose concentrations less than 0.3 mM, Δb* gradually increased with increasing glucose concentration and was saturated within 5 minutes after the start of glucose detection at the higher concentration. The corresponding color variations every 5 minutes (Figure 3a, upper inset) and images of the tested electrodes (Figure 3a, right inset) were also presented to visually illustrate the results. In contrast, the Δb* of the thick PB electrode (447 nm thick) showed precise responses in high-glucose solutions but low sensitivities and overlapped Δb* were observed at glucose concentrations below 0.5 mM (Figure 3b). The above behaviors of the thin and thick PB electrodes can be explained by saturation and slow oxidation rate, respectively (Figure 3c). For the high glucose concentration, the Δb* of the thin PB electrode was quickly saturated owing to the fast kinetics. Although saturation could be prevented by increasing the PB thickness, the diffusion of Na^+ and K^+ ions became sluggish compared with the diffusion in the thin PB electrode, resulting in slower

oxidation and undetectable variations in color change at low glucose levels after 20 minutes. Therefore, to widen the sensing range, four independent PB electrodes with thicknesses of 144, 238, 447, and 1082 nm (denoted as T_1, T_2, T_3, and T_4, respectively) were electrodeposited on the surface of the ITO-deposited contact lens, as shown in the scanning electron microscopy (SEM) cross-sectional images (Figure S5).

Figure 3d illustrates the computational image processing of the smart contact lens. Captures of the smart contact lens taken before and after glucose sensing were transferred to the computer for evaluation of the CIELAB color space parameters (L*, a*, and b*) via image processing. The regions of interest (ROI) detected for analysis were four PB electrode circular patterns, which were located via Canny edge detection and the Circle Hough transform algorithms (Figure S6). The target patterns were circled with green curves with different centers, and the corresponding L*, a*, and b* were calculated automatically. Each algorithm is detailed in Supplementary Note 1. In practical usage, these processes can be performed using a smartphone with the designed app.

To evaluate the optimal response time of the designed glucose sensor, the Δb^* of each electrode was examined for various response times from 5 to 30 minutes under both normal (0.2 mM) and high (0.9 mM) glucose conditions (Figure 3e). Despite the different reaction rates at distinct glucose levels and PB electrode thicknesses, the Δb^* of all tested PB electrodes exhibited steady responses after 20 minutes, indicating that the overall color change could be assessed after 20-minute processing. Inset photographs in Fig. 3e display the contact lens during image processing before and after 20-minute immersion in 0.2 and 0.9 mM glucose solutions. Processing images and Δb^* of the contact lens recorded at 5-minute intervals in 0.2 and 0.9 mM glucose solutions are presented in Figure S7, Table S1, and Table S2.

The responses of Δb^* to various glucose concentrations in tear at both normal (0.16 to 0.5 mM) [38] and high (0.9 mM) [39] levels within 20 minutes are illustrated in Figure 3f, and the inset color map reflects the corresponding color status of each electrode in diverse cases. With

the increasing glucose concentration of tear fluids, the Δb* between the initial and after-monitoring electrodes generally increased, resulting in larger color shifts from transparent to blue. Therefore, the various glucose concentrations were visibly indicated via the displayed color differences. Photographs of each electrode recorded every 5 minutes in solutions with different glucose concentrations are presented in Figure S8. According to the results, electrode T_1 exhibited effective distinctiveness in low-glucose solutions, while electrode T_4 showed more pronounced Δb* in high-glucose solutions, which were consistent with the previous single-electrode results. Hence, a wide range of tear glucose concentrations can be covered by such a multi-thickness electrode contact lens design. The color changes of the smart contact lens at normal (0.16 mM) and high (0.9 mM) glucose concentrations are compared in Supplementary Video 1.

Because human tears contain various interfering molecules in addition to glucose, selectivity assessments were verified by amperometric response tests and Δb* in the four PB electrodes. Additions of biologically relevant concentrations of ascorbic acid, lactate, and urea [14, 31] into a tear-like solution containing 0.145 M NaCl and 0.024 M KCl resulted in negligible changes in Δb. In contrast, the application of 0.2 mM glucose resulted in an increase of ~0.61 μA in the current of the amperometric test and a significant increase in the Δb* of the PB electrodes (Figure S9 and Supplementary Note 2).

The relationship between the corresponding glucose level and Δb* of each electrode acquired from the images captured at the initial and 20-minute intervals was developed by multi-linear regression of machine learning. The average glucose levels under diverse conditions with different electrode combinations were predicted using piecewise functions (Table S3, Figure S10). According to the algorithm, thinner electrodes played dominant roles at glucose concentrations lower than 0.3 mM, while thicker electrodes determined glucose concentrations over 0.5 mM. These conclusions are consistent with the previous multi-electrode

design hypothesis. Further explanations of the code during operations are provided in Supplementary Note 3.

In addition, the Δb^* electrode T_1 and T_2 at low glucose levels were examined to investigate the detection limit of the sensor (Figure S11). Both electrodes exhibited a distinguishable change at glucose concentrations down to 0.05 mM, indicating that the power-free contact lens achieved a detection limit of 0.05 mM.

The final predictions of the Δb^* of multiple electrodes obtained by the power-free contact lens agreed well with the results of the corresponding reference glucose concentrations, with the correlation coefficient $r = 0.99543$ (Figure 3g). Experimental datasets for training and testing were obtained in repeated experiments with different glucose conditions. The whole processing procedure is shown in Supplementary Video 2.

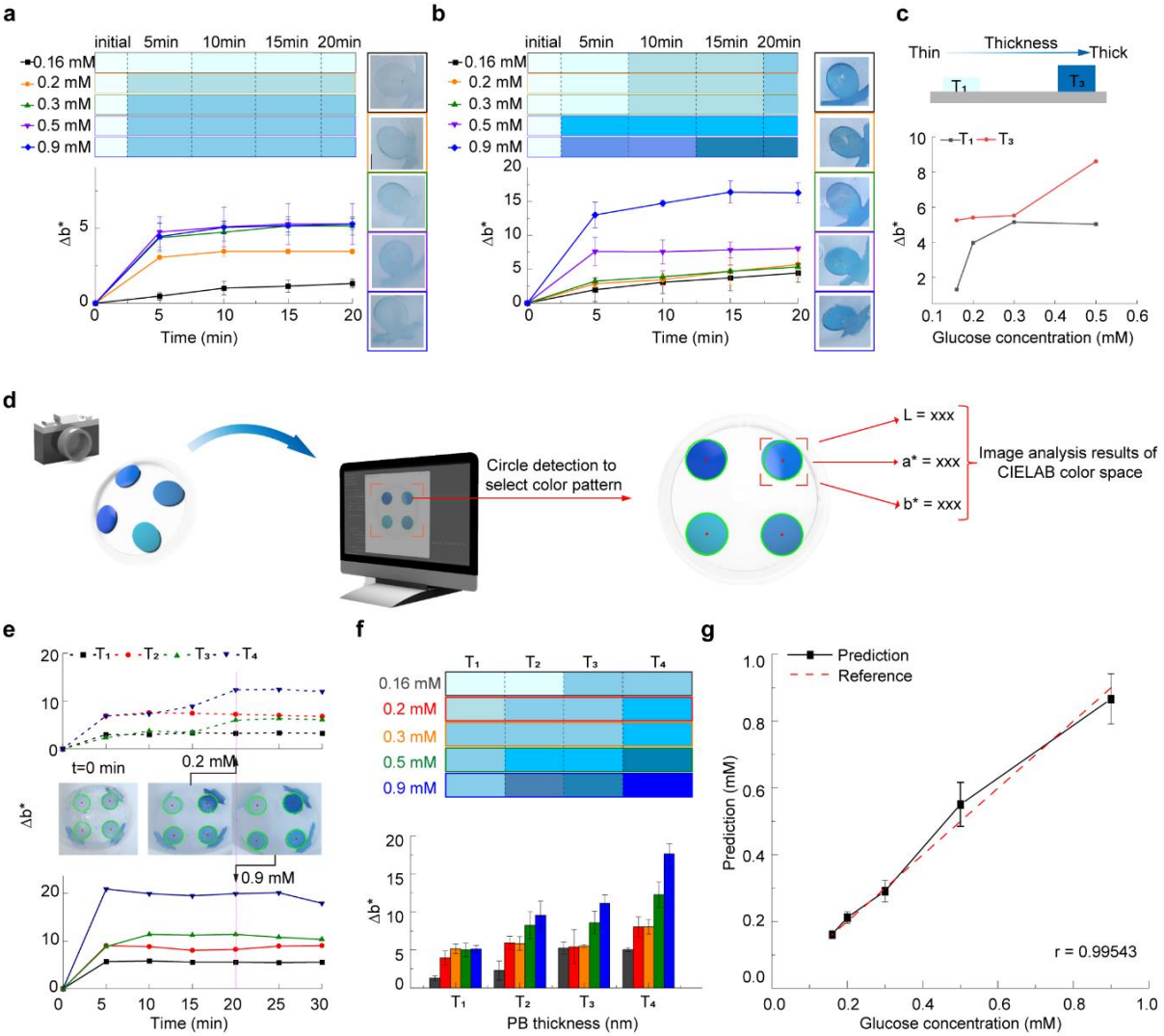

Figure 3. Color change detection with b* value differences. Δb* and experimental photographs of PB with **a)** T_1 (thin) and **b)** T_3 (thick) thicknesses recorded every 5 minutes. Insets are the corresponding color map and images of PB in different glucose solutions. **c)** Relationship between electrode color and glucose concentrations with different thicknesses. **d)** Schematic illustration of computational image processing. **e)** The trend of Δb* versus time of four PB electrodes with different thicknesses in 0.2 mM (below) and 0.9 mM (above) glucose solution. **f)** Δb* of four PB electrodes with different thicknesses after 20 minutes in various glucose concentrations. Inset is the corresponding color map of PB electrodes with corresponding thicknesses in different glucose solutions. **g)** Predicted results of the power-free smart contact lens.

2.3. Recycling capability evaluation

The initialization of the contact lens after detection to realize the repeatability of the sensor was achieved by the electrochemical method. The lens was stored in a conductive fluidic container, similar to that for the conventional contact lens. The container consisted of four conductive pads matching the four electrodes of the contact lens in both size and location. The consistent electrochemical characteristics of the PB electrodes after glucose sensing, confirmed by the CV testing results (Figure 2f), demonstrate the reversible glucose sensing of the smart contact lens. Therefore, the electrochemical reaction from PB to PW can be realized by applying the reduction potential to the contact lens electrodes via the conductive fluidic container, as illustrated in **Figure 4**a. Photographs of the pristine contact lens, the lens after detection and initialization, and the recycling experimental setup are presented in Figure 4b. Since all four pads of the container were completely connected with the coated conductive material, electrodes with different thicknesses of the contact lens could be reduced simultaneously. During the initialization, four PB electrodes performed as working electrodes, associated with the Ag/AgCl and platinum as the reference electrode and counter electrode, respectively. The overall setup of the initialization experiment under the reduction potential with the conductive container is presented in Supplementary Video 3. The repeatability was examined in vitro at a high glucose concentration (0.9 mM), and the predicted results exhibited stable response and showed good consistency with the reference value after four continuous cycles (Figure 4c). The insets of Figure 4c shows the contact lens of each cycle after initialization and glucose sensing. Standard deviations were evaluated to describe the consistency of the results during repeated experiments. After four continuous cycles, the standard deviation of the predicted results of the smart contact lens was 0.0462, indicating small divergences in the determined glucose levels among the different cycles. Besides, repeated detections after first-time use of the smart contact lens were conducted in 0.9 mM glucose solutions after 5 days, 10 days, and 15 days, respectively to evaluate the long-term stability, as indicated in Figure 4d. Negligible variations

with a standard deviation of 0.025 in predicted glucose levels occurred even after a 15-day duration, and the results agreed well with the theoretical concentrations, reflecting acceptable stabilities in both PB and GOX layers with the protection of the Nafion membrane in ambient environments. The inset graph of Figure 4d illustrates the Δb* of each electrode after 0, 5, 10, and 15 days after the first use of the contact lens, respectively. Although electrodes T_1 and T_4 exhibited a noticeable decay over time, the influences of the variations on the final predictions were negligible because the decreased Δb* were still located in the tolerance ranges. Further optimizations on extending the stability of the biosensors like pre-treatment of the pristine electrodes for robust PB electrodeposition will be investigated.

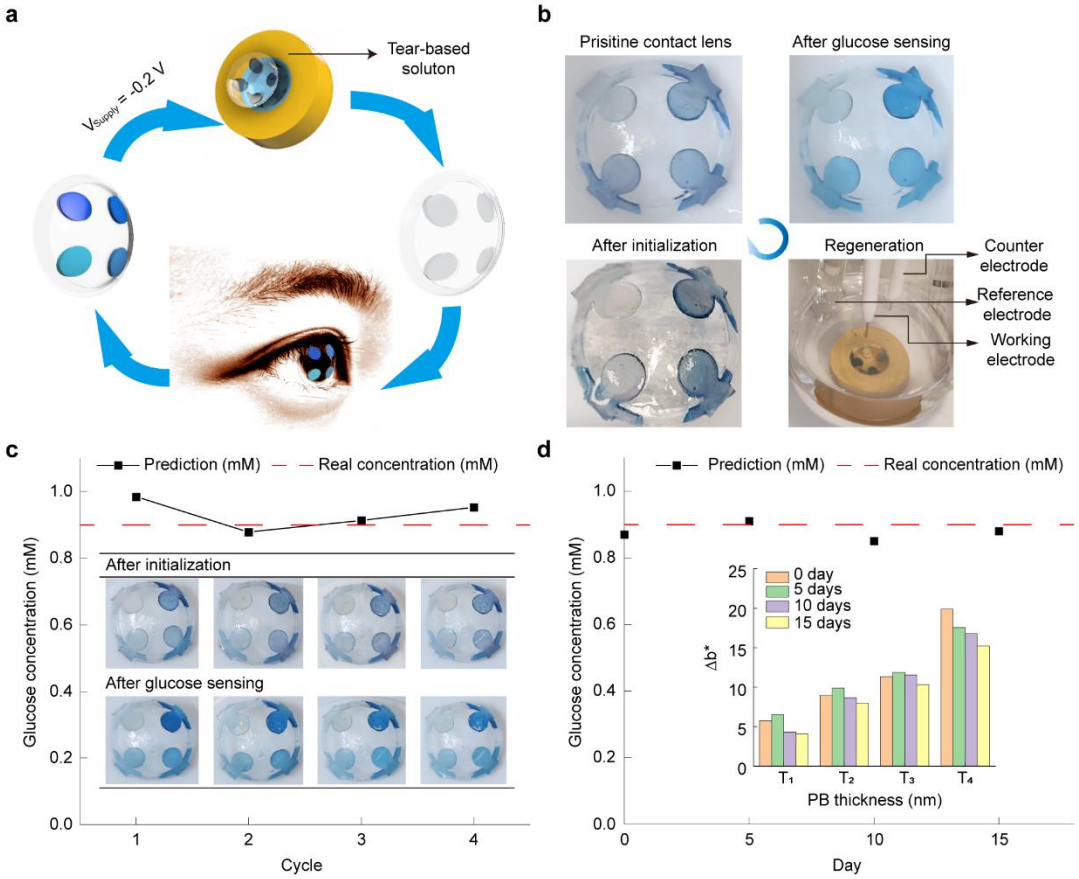

Fig. 4 Recycle and long-term test of power-free smart contact lens. **a)** Schematic illustration of the recycling process. **b)** Photographs of each state during initialization processes. **c)** Predicted result of the power-free smart contact lens system in 0.9 mM glucose solution in 4 cycles. Inset photographs indicate the initial and final state of each cycle. **d)** Predicted results of the second time use of contact lens after 0 days/5 days/10 days/15 days, respectively. The

inset graph shows Δb* of each electrode at the second time use after 0 days/5 days/10 days/15 days, respectively.

3. Conclusion

In this paper, we demonstrated a power-free smart contact lens sensor based on the electrochemical reactions of biocompatible electrochromic electrodes for noninvasive glucose sensing and direct data transmission via color change without a power supply and external wireless transmission. The absence of the power supply and wireless transmission allows for the simple and cost-effective manufacturing of the device. The biocompatibility of the PB electrodes was preliminarily evaluated in our previous study through cytotoxicity tests on MDA-MB-231 cells [16]. Additionally, tears contain all the necessary ions for redox reactions of PB during glucose sensing, eliminating the need for additional electrolytes. These findings support the application of PB as a safe and promising material in the proposed power-free contact lens. Multiple electrodes with different thicknesses were embedded in the smart contact lens for broad-range sensing, and the lens yielded acceptable results under diverse glucose conditions. Image processing and machine learning algorithms were applied for precise prediction, with a correlation coefficient r = 0.99543 and an improved detectable limit. However, it is important to consider the dynamics of tear glucose concentrations, especially in situations where glucose levels fluctuate rapidly such as after meals. Significant associations have been observed between tear glucose and blood sugar levels, suggesting that the sampling time of blood sugar level tests can serve as a reference. Therefore, providing suggestions on the optimal usage time that is applied for blood sugar level tests such as before meals, before bedtime, or 2 hours after meals for the sensor can greatly enhance the practicality and usability for future daily use. The implementation of the Nafion membrane improved the stability and immobilization of enzyme-covered electrode materials after specific analyte sensing, offering possibilities for the reusability and long-term storage of the contact lens sensor, with acceptable standard deviations of 0.0462 and 0.025 for four continuous cycles and for an interval of several

days, respectively. In comparison to previous power-consuming methods, our sensor achieves acceptable predicted results with a similar correlation coefficient (0.99543 vs. 0.99910 [40]) without power consumption. Furthermore, compared to reported colorimetric sensing methods, our sensor exhibits a lower detection limit (0.05 mM) and demonstrates the potential for repeatability and long-term storage. Currently, the lens can be used at least 4 times before disposal with the protection of the Nafion membrane. However, challenges remain in terms of the enzyme's activity and the degradation of PB electrodes in neutral or alkaline solutions. The enzyme's lifespan can be prolonged by storing it below room temperature, and the stability of PB electrodes can be enhanced through various methods, such as improving PB electrodeposition conditions [41], applying post-treatment techniques [42], utilizing external protective polymer or surfactant films [43], and employing electrochemical ion insertion methods for PB modification [44]. Additionally, further optimizations of the sensor and code of image analysis are necessary to enhance the practicality and usability of the sensor for future daily use. We envision that such power-free wearable technology has potential application for the monitoring of various metabolites in addition to glucose for the safer and more convenient early diagnosis of various diseases.

4. Methods

Materials: Potassium hexacyanoferrate ($K_3Fe(CN)_6$), iron (III) chloride ($FeCl_3$), hydrochloric acid (37%, HCl), D-(+)-glucose, glucose oxidase (GOX, from Aspergillus niger), Nafion (20wt%)), ammonium hydroxide solution (NH_4OH), ethanol, hydroxyethyl methacrylate (HEMA), 2-hydroxy-2-methylpropiophenone, ethylene glycol dimethacrylate (EGDMA), sodium chloride (NaCl), and potassium chloride (KCl) were purchased from Sigma-Aldrich. Urea (Molecular biology grade) was purchased from Vivantis. Ascorbic acid (AA) was obtained from the Blackmores BIO C 1000. The conductive material indium tin oxide (ITO), titanium (Ti), and gold (Au) targets were obtained from LEE & LIM INTERNATIONAL.

Dragon skin 20 was purchased from Mold Creative (S) Pte Ltd. Clear V4 resin was purchased from Formlabs.

Design of the smart contact lens: Both the smart contact lens with four equal spaces on the surface for electrode deposition and sensing and the conductive container for initialization were designed using the computer-aided design (CAD) software Fusion 360. The height of the contact lens was set as 3.6 mm, with a 14.5 mm outer diameter and 12.5 mm inner diameter. The sketch of the surface region for each electrode was in a circle shape with a diameter of 3.5 mm, leaving a 5 mm hole at the center.

Fabrication of the biosensor: Deposition of 250 nm ITO on the 3D-printed contact lens was conducted by the versatile sputter coater (Quorum Q300T D plus) under a 120-mA current with shadow masks to block conductive connections between different electrodes. Each electrode was prepared by electrodeposition on an area of approximately 9.62 mm^2 circle pad at a current of $-50\ \mu A$ in the mixture solution consisting of 20 mM $K_3Fe(CN)_6$, 20 mM $FeCl_3$, and little amount of HCl to create an acid environment. The thickness of the electrode was determined by the electrodeposited time, with 15, 30, 70, and 150 seconds for each electrode. The enzyme solution GOX (1U/2 μL) was prepared in deionized (DI) water. A volume of 6.8 μL was applied to each PB electrode and dried at room temperature for 1 day to modify the glucose biosensor, followed by covering a 2-layer 0.3 wt% Nafion solution, with a volume of 6.8 μL in each layer to protect the modified electrodes. The 0.3 wt% Nafion solution was obtained by diluting 20 wt% Nafion solution in ethanol, and the pH was adjusted to 7 with ammonium hydroxide solution.

Preparation of the hydrogel and lens formation: The hydrogel solution was prepared by mixing HEMA, DI water, 2-hydroxy-2-methylpropiophenone, and EGDMA in a weight ratio of 5:3:0.1:0.1. The lab-made mold for contact lens formation was formed with Dragon skin 20 eco flex part A and part B solution in a weight ratio of 1:1 in the oven at 60 °C for 30-minute drying.

The sensor-embedded contact lens was then put in the curvature shape mold filled with hydrogel solution and polymerized by UV illumination with a wavelength of 365 nm for 5 minutes.

Design of the conductive container: The conductive container was designed in a cylinder shape in the size of 15 mm (diameter) × 10 mm (height), with a groove designed in the same profile as the contact lens for perfect matches in electrical contact connections during the supplement in the reduction potential. 5 nm adhesive layer Ti and 50 nm conductive layer Au were deposited on the surface of the 3D-printed container using the sputter sequentially, under a current of 100 mA and 50 mA, respectively.

In vitro characterization of the sensors: In vitro characterizations were conducted in a tear-like aqueous electrolyte solution consisting of 0.145 M NaCl and 0.024 M KCl with various glucose concentrations to evaluate the performances of the biosensor. The amperometric responses were obtained at an applied potential of −0.2 V (Figure. S4b). The prediction of the glucose biosensors was achieved by the generated linear relationships using differences of b* values of each electrode captured before and after glucose detection as independent inputs. All experiments were conducted at the surface temperature of the eyeball, ranging between 33 and 35℃, and the photographs were taken by Canon EOS 5D Mark iv in the condition of 1/5s shutter speed, f/13.0 aperture value, and 100 ISO under the ambient light environment. The accuracy was examined by calculating the correlation coefficient r. The repeatability was demonstrated at 0.9 mM glucose level, and the initialization was realized by the three-cell system with the conductive container at a potential of −0.2 V, as described in the previous chapter. The performance of the reproducibility and consistency of the glucose biosensor was examined and presented with precision.

Supporting Information

Supporting Information is available from the Wiley Online Library or from the author.

Acknowledgments

The authors would like to acknowledge the Facility for Analysis, Characterization, Testing and Simulation (FACTS), Nanyang Technological University, Singapore, for use of their SEM facilities. S.W.L. acknowledges the support by the National Research Foundation, Prime Minister's Office, Singapore under its NRF-ANR Joint Programme (NRF2019-NRF-ANR052 KineHarvest).

Author contributions

Z.L. and S.W.L. conceived the research and designed experiments. Z.L., J.Y., X.L., and S.W. L analyzed and interpreted data. Z.L. and M.K contributed to the processing codes of the smart contact lens. J.L., D.L., and A.W. assisted in experimental work. Z.L. and S.W.L. wrote the manuscript and all authors reviewed and revised the manuscript.

Competing interest

The authors declare no competing interests.

Data availability

The main supporting research data are available within the graphs, tables, and Excel files in both the paper and Supplementary Information. Both testing and training datasets were generated by conducted experimental outcomes.

References

[1] N. G. Forouhi, N. J. Wareham, *Medicine.* **2010**, *38*, 602.

[2] U. Alam, O. Asghar, S. Azmi, R. A. Malik, *Handbook of Clinical Neurology*, D. W. Zochodne, R. A. Malik, Elsevier **2014**.

[3] D. Olczuk, R. Priefer, *Diabetes Metab Syndr.* **2018**, *12*, 181.

[4] D. Bruen, C. Delaney, L. Florea, D. Diamond, *Sensors.* **2017**, *17*, 1866.

[5] A. J. Bandodkar, J. Wang, *Trends Biotechnol.* **2014**, *32*, 363.

[6] S. Patel, H. Park, P. Bonato, L. Chan, M. Rodgers, *Journal of NeuroEngineering and Rehabilitation.* **2012**, *9*, 21.

[7] J. Andreu-Perez, D. R. Leff, H. M. Ip, G. Z. Yang, *IEEE Trans Biomed Eng.* **2015**, *62*, 2750.

[8] W. Jia, A. J. Bandokar, G. Valdés-Ramírez, J. R. Windmiller, Z. Yang, J. Ramírez, G. Chan, J. Wang, *Anal Chem.* **2013**, *85*, 6553.

[9] W. Gao, S. Emaminejad, H. Y. Y. Nyein, S. Challa, K. Chen, A. Peck, H. M. Fahad, H. Ota, H. Shiraki, D. Kiriya, D-H. Lien, G. A. Brooks, R. W. Davis, A. Javey, *Nature.* **2016**, *529*, 509.

[10] Q. Yan, B. Peng, G. Su, B. E. Cohan, T. C. Major, M. E. Meyerhoff, *Anal Chem.* **2011**, *83*, 8341.

[11] J. Park, J. Kim, S. -Y. Kim, W. H. Cheong, J. Jang, Y. -G. Park, K. Na, Y. -T. Kim, J. -H. Heo, C. Y. Lee, J. H. Lee, F. Bien, J-U. Park, *Sci Adv,* **2018**, *4*, 9841.

[12] N. Thomas, I. Lähdesmäki, B. A. Parviz, *Sensors and Actuators B: Chemical.* **2012**, *162*, 128.

[13] J. Kim, M. Kim, M. -S. Lee, K. Kim, S. Ji, Y-T. Kim, J. Park, K. Na, K. -H. Bae, H. K. Kim, F. Bien, C. Y. Lee, J. -U. Park, *Nat Commun,* **2017**, *8*, 14997.

[14] D. H. Keum, S. -K. Kim, J. Koo, G. -H. Lee, C. Jeon, J. W. Mok, B. H. Mun, K. J. Lee, E. Kamrani, C. -K. Joo, S. Shin, J. -Y. Sim, D. Myung, S. H. Yun, Z. Bao, S. K. Hahn, *Sci Adv.* **2020**, *6*, 3252.

[15] H. Mirzajani, F. Mirlou, E. Istif, R. Singh, L. Beker, *Biosens Bioelectron.* **2022**, *197*, 113761.

[16] J. Yun, Y. Zeng, M. Kim, C. Gao, Y. Kim, L. Lu, T. T. -H. Kim, W. Zhao, T. -H. Bae, S. W. L, *Nano Lett.* **2021**, *21*, 1659.

[17] H. Lee, S. Kim, K.-B. Kim, and J.-W. Choi, *Nano Energy.* **2018**, *53*, 225.

[18] R. C. Reid, S. D. Minteer, B. K. Gale, *Biosens Bioelectron.* **2015**, *68*, 142.

[19] M. Falk, V. Andoralov, Z. Blum, J. Sotres, D. B. Suyatin, T. Ruzgas, T. Arnebrant, S. Shleev, **2012**, *37*, 38.

[20] A. Vásquez Quintero, R. Arai, Y. Yamazaki, T. Sato, H. De Smet, *Advanced Materials Technologies.* **2020**, *5*, 2000702.

[21] L. R. Chen, G. Shaker, S. Safavi-Naeini, *2017 IEEE International Symposium on Antennas and Propagation & USNC/URSI National Radio Science Meeting.* **2017**, 1293.

[22] M. Kim, I. D. Jung, Y. Kim, J. Yun, C. Gao, H. -W. Lee, S. W. L, *Sensors and Actuators B: Chemical.* **2020**, *322*, 28601.

[23] R. Moreddu, J. S. Wolffsohn, D. Vigolo, A. K. Yetisen, *Sensors and Actuators B: Chemical.* **2020**, *317*, 128183

[24] H.-J. Jeon, S. Kim, S. Park, I. -K. Jeong, J. Kang, Y. R. Kim, D. Y. Lee, E. Chung, *Nano Letters.* **2021**, *21*, 8933.

[25] F. Charbgoo, M. Ramezani, M. Darroudi, *Biosensors and Bioelectronics.* **2017**, 96, 33.

[26] C. Xu, X. Qu, *NPG Asia Materials.* **2014**, *6*, 90.

[27] A. A. Karyakin, O. V. Gitelmacher, E. E. Karyakina, *Anal Chem.* **1995**, *67*, 2419.

[28] X. Wang, H. Gu, F. Yin, Y. Tu, *Biosensors and Bioelectronics.* **2009**, *24*, 1527.

[29] W. Zhang, D. Ma, J. Du, *Talanta.* **2014**, *120*, 362.

[30] A. Chaudhary, T. Ghosh, D. K. Pathak, S. Kandpal, M. Tanwar, C. Rani, R. Kumar, *IET Nanodielectrics.* **2021**, *4*, 165.

[31] M. Shokouhimehr, E. S. Soehnlen, A. Khitrin, S. Basu, S. D. Huang, *Inorganic Chemistry Communications.* **2010**, *13*, 58.

[32] N. A. Sitnikova, A. V. Borisova, M. A. Komkova, A. A. Karyakin, *Analytical Chemistry.* **2011**, *83*, 2359.

[33] J. Ahn, S. Kim, S.-i. Jeon, C. Lee, J. Lee, J. Yoon, *Desalination,* **2021**, *500*, 114778.

[34] J. J. García-Jareño, J. Navarro-Laboulais, F. Vicente, *Electrochimica Acta.* **1996**, *41*, 2675.

[35] D. O. Ojwang, M. Swensson, C. Njel, R. Mogensen, A. S. Menon, T. Ericsson, L. Häggström, J. Maibach, R. Brant, *ACS Applied Materials & Interfaces.* **2021,** *13*, 10054.

[36] J. Ahn, S. Kim, S. -I. Jeon, C. Lee, J. Lee, J. Yoon, *Desalination.* **2021**, 500, 114778.

[37] J. -M. Noël, J. Médard, C. Combellas, F. Kanoufi, *ChemElectroChem.* **2016**, *3*, 1178.

[38] H. Yao, A. J. Shum, M. Cowan, I. Lahdesmaki, B. A. Parviz, *Biosens Bioelectron.* 2011, *26*, 3290.

[39] D. K. Sen, G. S. Sarin, *The British journal of ophthalmology*, **1980**, *64*, 69

[40] S. -K. Kim, G. -H. Lee, C. Jeon, H. H. Han, S. -J. Kim, J. W. Mok, C. -K. Joo, S. Shin, J. -Y. Sim, D. Myung, Z. Bao, S. K. Hahn, *Advanced Materials*. **2022**, *34*, 2110536.

[41] A. A. Karyakin, *Electroanalysis*. **2001**, *13*, 813.

[42] Z. Wang, H. Yang, B. Gao, Y. Tong, X. Zhang, L. Su, *Analyst.* **2014**, *139*, 1127.

[43] N. A. Sitnikova, A. V. Borisova, M. A. Komkova, A. A. Karyakin, *Analytical Chemistry.* **2011**, *83*, 2359.

[44] D. Iveković, H. V. Trbić, R. Peter, M. Petravić, M. Čeh, B. Pihlar, *Electrochimica Acta.* **2012**, *78*, 452.